Atmos. Chem. Phys. Discuss., 10, 30857–30891, 2010
www.atmos-chem-phys-discuss.net/10/30857/2010/
doi:10.5194/acpd-10-30857-2010


Atmospheric Chemistry and Physics Discussions



# The two faces of cirrus clouds

**D. Barahona**[1,*] **and A. Nenes**[1,2]

[1]School of Chemical and Biomolecular Engineering, Georgia Institute of Technology, Atlanta, GA, USA
[2]School of Earth and Atmospheric Sciences, Georgia Institute of Technology, Atlanta, GA, USA
[*]now at: NASA Goddard Space Flight Center, Greenbelt, MD, USA

Received: 28 November 2010 – Accepted: 6 December 2010 – Published: 20 December 2010

Correspondence to: A. Nenes (athanasios.nenes@gatech.edu)

Published by Copernicus Publications on behalf of the European Geosciences Union.

## Abstract

Low ice crystal concentration and sustained in-cloud supersaturation, commonly found in cloud observations at low temperature, challenge our understanding of cirrus formation. Heterogeneous freezing from effloresced ammonium sulfate, glassy aerosol, dust and black carbon are proposed to cause these phenomena; low updrafts however is required for cirrus characteristics to agree with observations and is at odds with the gravity wave spectrum in the upper troposphere. Instead, background temperature fluctuations can establish a “dynamical equilibrium” between ice production and sedimentation loss that explains low temperature cirrus properties. This newly-discovered state is favored at low temperatures, does not require heterogeneous nuclei to occur, and is insensitive to their presence. Our understanding of cirrus clouds and their role in anthropogenic climate change is reshaped, as the type of dynamical forcing will set these clouds in one of two “preferred” microphysical regimes with very different susceptibility to aerosol.


## 1 Introduction

Cirrus clouds are composed of ice crystals that form at high altitudes and temperatures typically below 235 K (Pruppacher and Klett, 1997). They play a key role in climate by modulating the planetary radiative balance (Liou, 1986) and heat transport in the upper troposphere (Ramanathan and Collins, 1991). They strongly impact water vapor transport across the tropopause level (Jensen and Pfister, 2004) and play an important role in lower stratospheric chemistry (Peter, 1997). Cirrus may be affected by aircraft emissions (Seinfeld, 1998) and long range transport of pollutants (Fridlind et al., 2004), and are an important (but highly uncertain) component of anthropogenic climate change.

A key microphysical parameter required for understanding the climate impact of cirrus is their concentration of ice crystals, $N_c$. It is known that at temperatures between 200 K and 235 K cirrus ice crystals form primarily by homogenous freezing of





ACPD

10, 30857–30891, 2010

supercooled deliquesced aerosol (DeMott et al., 2003; Heymsfield and Sabin, 1989), which occurs if the saturation ratio with respect to ice, $S$, (i.e., the ratio of water vapor partial pressure to its equilibrium value over ice) reaches a characteristic threshold value, $S_{hom}$ (Koop et al., 2000). Heterogeneous freezing of water upon existing aerosol particles (termed "ice nuclei", IN) can also occur (at $S$ lower than $S_{hom}$) and contribute to ice crystal concentrations (DeMott et al., 2003; Froyd et al., 2009). The level of water vapor supersaturation (i.e., $S-1$) is the thermodynamic driver for ice formation, and is generated by expansion of air parcels forced by large scale dynamics, gravity waves, and small scale turbulence (Kim et al., 2003).

At temperatures below 200 K, the simple conceptual model for cirrus presented above is at odds with observations (Jensen et al., 2010; Krämer et al., 2009; Peter et al., 2006). Temperature fluctuations from mesoscale gravity waves are common at high altitudes and can produce localized vertical motion with updraft velocity as large as $1\,\mathrm{m\,s^{-1}}$ (Bacmeister et al., 1999; Herzog and Vial, 2001; Jensen and Pfister, 2004; Sato, 1990). Homogeneous freezing driven by this motion would produce high ice crystal number concentration, $N_c$, between 1 and $10\,\mathrm{cm^{-3}}$ near the tropopause (Fig. 1). Such high concentrations however are not observed; $N_c$ remains low, sometimes even lower ($0.005$–$0.2\,\mathrm{cm^{-3}}$) than concentrations observed in weak updraft zones at cold temperatures (Krämer et al., 2009; Lawson et al., 2008). This "low $N_c$" paradox is accompanied by other unexplained phenomena, such as low supersaturation relaxation times (Krämer et al., 2009), which in turn leads to sustained supersaturation levels inside clouds (i.e., "the supersaturation puzzle", Gao et al., 2004), high clear-sky supersaturation (Jensen et al., 2005), and broad ice crystal size distributions (i.e., large crystal sizes, Jensen et al., 2008). These phenomena occur despite the strong dynamical forcing and the ample amounts of deliquesced aerosol available for homogeneous freezing. Suppressed freezing by organics (Murray, 2008), slow water vapor transfer to the ice phase (Gao et al., 2004; Magee et al., 2006), and freezing to cubic instead of hexagonal ice (Murray et al., 2005), have been proposed to explain these features. These mechanisms however only act under specific conditions and cannot



ACPD
10, 30857–30891, 2010

explain the low $N_c$ and high $S$ coexisting in low temperature cirrus clouds (Peter et al., 2006). Lacking the predictive understanding of such phenomena hinders the ability of climate models to capture the climate effects of cirrus clouds and their response to anthropogenic perturbations.

Recently, heterogeneous freezing of IN as the main path of cirrus formation has been proposed to explain the features of cirrus clouds at low temperature (Abbatt et al., 2006; Jensen et al., 2010; Murray et al., 2010). Owing to their ability to freeze at much lower supersaturation than homogeneous freezing requires, IN can deplete water vapor, reduce supersaturation and inhibit homogeneous freezing; this can drastically reduce the number of ice crystals that forms in the cirrus (Barahona and Nenes, 2009a). Much of the anthropogenic impact on cirrus clouds and climate is thought to occur through this IN-$N_c$ feedback mechanism (Lohmann and Feichter, 2005). In this work we analyze the range of conditions for which heterogeneous freezing may explain the features of cirrus clouds at low temperature, and propose an alternative view (based on a statistical description of cirrus formation and evolution) in which the interplay of temperature fluctuations, and ice crystal production and sedimentation leads to previously unidentified cirrus states of low ice crystal concentration and sustained high supersaturation.

## 2 Heterogeneous freezing at low temperature

The impact of IN on $N_c$ depends on their concentration, $N_{IN}$. If too low ($N_{IN}<1\times10^{-4}\,cm^{-3}$), a negligible impact is seen on $N_c$, as too few (heterogeneously-frozen) ice crystals form to quench supersaturation below the homogeneous freezing threshold (Barahona and Nenes, 2009a). Low $N_c$ favors large crystal size and therefore heterogeneously frozen ice crystals may sediment out of the cloud layer before significantly modifying $S$ (Spichtinger and Gierens, 2009a). When $N_{IN}$ approaches a characteristic "limiting" concentration (which depends on updraft velocity, the IN freezing threshold and size), $N_{lim}$, supersaturation is quenched, homogeneous freezing is depressed, and $N_c$ decreases steeply (Barahona and Nenes, 2009a). For $N_{IN}\geq N_{lim}$, homogeneous



ACPD
10, 30857–30891, 2010

nucleation is inhibited and $N_c = N_{IN}$. Thus, $N_{lim}$ is the minimum $N_c$ that can form in an active nucleation zone in a freshly-formed cirrus cloud (Barahona and Nenes, 2009a) and presents the maximum reduction in $N_c$ possible from IN.

Simulations show that if $N_{IN}$ is always very close to $N_{lim}$, competition between homogeneous and heterogeneous freezing could yield $N_c$ close to observations (Fig. 1; the simulation approach is described in Sect. 3.3). This requires $N_{IN} \sim 0.1\,cm^{-3}$, which is 20-fold higher than typically measured dust concentrations ($\sim 0.05\,cm^{-3}$) at the tropopause level (Froyd et al., 2009). Ammonium sulfate aerosol is present at much higher concentrations than dust, and can serve as IN (Abbatt et al., 2006; Wise et al., 2010) if a fraction of them is effloresced (which is possible, given that it deliquesces at ~90% relative humidity) (Fountoukis and Nenes, 2007; Shilling et al., 2006).

To inhibit homogeneous freezing and reproduce observations of $N_c$, the concentration of ammonium sulfate IN needs to be within 10% of $N_{lim}$; if concentrations fall below $0.9\,N_{lim}$, homogeneous freezing is triggered and predicted $N_c$ is significantly above observations (Fig. 1). If higher concentration than $N_{lim}$ is present, homogeneous freezing is completely suppressed, but too many crystals still form (Barahona and Nenes, 2008). In fact, if all ammonium sulfate is available as IN, $N_c$ from heterogeneous freezing and pure homogeneous freezing are always comparable (Fig. 2), because crystals formed from ammonium sulfate IN are very small (with size close to the dry aerosol; 0.02–0.05 µm, Froyd et al., 2009) and grow too slowly to quench supersaturation before a large fraction of the aerosol freezes heterogeneously. $N_c$ is within observed values only if the average size of crystals at the point of freezing is 2 µm or larger (Fig. 2), which is too large for upper tropospheric aerosol (Froyd et al., 2009). Experimental studies suggest that heterogeneous freezing of ammonium sulfate IN at $T \sim 240\,K$ can be very selective (about 1 in $10^5$ particles nucleate ice, Shilling et al., 2006). If the same selectivity maintains at lower $T$, too few IN would be available to prevent homogeneous freezing (therefore resulting in high $N_c$). Higher nucleation selectivity (e.g., about 1 in $10^2$ particles actively nucleating ice) would result in complete inhibition of heterogeneous freezing and still maintain $N_c$ close to observations (not shown). A pure





ACPD
10, 30857–30891, 2010

heterogeneous freezing scenario however implies a maximum supersaturation below 20% (Fig. 3b), which is at odds with observations of relative humidity that suggest supersaturation between 30% and 70% (Froyd et al., 2009; Krämer et al., 2009). Hence, with the exception of a remarkably constant concentration of ammonium sulfate IN ($0.1\pm0.01\,\text{cm}^{-3}$) or exceptionally large concentration of dust, heterogeneous IN cannot explain the low $N_c$ and high $S$ observed at high-level cirrus.

The freezing fraction of organic glassy aerosol is much lower than that of ammonium sulfate and can maintain $N_{IN}$ close to $N_{lim}$ (hence yield low $N_c$, Fig. 3) for clouds forced by low updraft velocity up to $15\,\text{cm}\,\text{s}^{-1}$ (Murray et al., 2010). At larger updrafts however, homogeneous freezing is triggered, producing high $N_c$ (Fig. 3). The onset of homogeneous freezing occurs at even lower $u$ for colder temperatures. Predominance of heterogeneous freezing from glassy IN would also imply $S$ mostly below 30% (Barahona et al., 2010a; Murray et al., 2010), at odds with in situ observations (Krämer et al., 2009). All together, this implies that in the presence of (ubiquitous) $T$ fluctuations, the presence of glassy IN can contribute but not fully account for the observed characteristics of cirrus.

## 3 Parcel ensemble model

Ice falling though active freezing zones (typically located at the top of the cirrus layer, Spichtinger and Gierens, 2009b) in clouds consume water vapor and can inhibit homogeneous freezing much like IN do (Kay et al., 2007; Spichtinger and Gierens, 2009b). Their effectiveness depends on their residence time in freezing zones, hence depends on their size. Large ice crystals tend to quickly fall out of freezing zones and have limited effect on new ice formation events; small crystals (typically those with terminal velocity, $u_{term}$, less or equal to the mean updraft $\overline{u}$ of the cirrus layer) fall slowly and can remain long enough in the upper part of the cloud to affect new freezing events. This suggests that at low temperatures preexisting (and typically small, Krämer et al., 2009) ice crystals may locally dehydrate the freezing zone sufficiently to inhibit the formation





ACPD
10, 30857–30891, 2010

of new ice. The rate of crystal production is not uniform through the freezing zone, as "local" saturation ratio, $S$, and updraft velocity, $u$ (defined at the scale of individual cloud "parcels" $\sim 10^0$–$10^2$ m, Pruppacher and Klett, 1997) may be affected by fluctuations in wind speed and temperature induced by gravity waves (Kärcher and Haag, 2004; Kim et al., 2003). These internal $S$ variations are usually neglected in cirrus cloud studies on the basis that the long-term evolution of the cloud is determined by the mean values of $S$ and $u$. Below we show that accounting for them can profoundly impact the state and microphysical evolution of the cirrus cloud.

The main processes affecting the evolution of $N_c$ and mean saturation ratio, $S_o$, within a cirrus layer are the freezing of new ice, the sedimentation of existing ice crystals, the lifting of air masses (which generates supersaturation), and the relaxation (i.e., mass transfer) of water vapor to/from the ice phase. The magnitude of each process can be expressed in terms of a characteristic timescale, i.e., $\tau_{fr}$, $\tau_{sed}$, $\tau_{lift}$, and $\tau_{rel}$ for freezing, sedimentation, lifting, and relaxation, respectively. Fluctuations in $S$ and $u$ can have a strong impact on all cloud processes; we therefore represent them in terms of a probability distribution centered about the cirrus-average saturation ratio, $S_o$, and vertical velocity, $\overline{u}$. The width of these probability distributions is largely determined by the mean amplitude of temperature fluctuations, $\delta T$ (Bacmeister et al., 1999; Hoyle et al., 2005; Kärcher and Burkhardt, 2008). If homogeneous freezing is the only ice production mechanism considered, the rate of ice production is given by the frequency with which $S$ exceeds the homogeneous freezing threshold (Kärcher and Burkhardt, 2008) times the length and intensity of each freezing event (hence $\tau_{fr}$) (Barahona and Nenes, 2008; Pruppacher and Klett, 1997). The same fluctuations also affect the local mass transfer rate between the ice and vapor phases, so that when averaged over the cloud, water deposition/sublimation occurs at an "effective" saturation ratio, $S_{eff}$, that may differ from $S_o$. From these considerations, simple equations can be derived that represent the evolution of $N_c$, $S_o$ in the cirrus (Sect. 3.1).





ACPD
10, 30857–30891, 2010

### 3.1 Evolution of saturation ratio

Supersaturation and crystal number in the cirrus cloud are determined using a "Lagrangian trajectory ensemble" approach. This involves determining the time-dependant state of $i$ homogeneous adiabatic Lagrangian "parcels" that move with a (time-dependant) vertical velocity, $u_i$; ensemble averaging of the parcel solutions (outlined below) give approximate equations that describe the time-dependant properties for the whole cirrus.

In the absence of ice nucleation, the rate of change of saturation ratio, $S$, within the $i$th Lagrangian parcel is given by (Barahona and Nenes, 2009b; Seinfeld and Pandis, 1998)

$$\frac{dS_i}{dt} = \alpha u_i S_i - \gamma \int_{D_{\min}}^{\infty} D_{c,i}^2 \frac{dD_{c,i}}{dt} n_{c,i}(D_c) dD_c \tag{1}$$

where $\alpha = \frac{g\Delta H_s M_w}{c_p R T^2} - \frac{g M_a}{RT}$ and $\gamma = \frac{\rho_i}{\rho_a}\frac{\pi}{2}\frac{M_a\, p}{M_w p_i^o}$, $\Delta H_s$ is the latent heat of sublimation of water, $g$ is the acceleration of gravity, $c_p$ is the heat capacity of air, $p_i^o$ is the ice saturation vapor pressure at $T$ (Murphy and Koop, 2005), $p$ is the ambient pressure, $M_w$ and $M_a$ are the molar masses of water and air, respectively, and $R$ is the universal gas constant, $\rho_i$ and $\rho_a$ are the ice and air densities, respectively, and $D_c$ is the volume-equivalent diameter of an ice particle (assuming spherical shape). $n_{c,i}(D_c)$ is the ice crystal size distribution in the $i$th parcel, and

$$\frac{dD_{c,i}}{dt} = \frac{G(S_i - 1)}{D_{c,i}} \tag{2}$$

where $G \approx \left[\frac{\rho_i RT}{4 p_i^o D_v' M_w} + \frac{\Delta H_s \rho_i}{4 k_a T}\left(\frac{\Delta H_s M_w}{RT} - 1\right)\right]^{-1}$, $k_a$ is the thermal conductivity of air, $D_v$ is the water vapor diffusion coefficient from the gas to ice phase. Substituting Eq. (2) into





ACPD
10, 30857–30891, 2010

Eq. (1) provides after evaluation of the integral,

$$\frac{dS_i}{dt} = \alpha u_i S_i - \frac{(S_i - 1)}{\tau_{\mathrm{rel},i}} \tag{3}$$

where $\tau_{\mathrm{rel},i} = (\beta N_{\mathrm{c},i} \overline{D}_{\mathrm{c},i})^{-1}$ is the relaxation time scale in the $i$th parcel, $\beta = \gamma G$, and, $N_{\mathrm{c},i}$, $\overline{D}_{\mathrm{c},i}$ are the concentration and mean size of ice crystals in the $i$th parcel, respectively.

Equation (3) provides the supersaturation "state" for every Lagrangian parcel considered in the ensemble. Knowledge of the distribution of $u_i$ (from the spectrum of gravity waves in the cirrus) can then be used to "drive" the parcels in the ensemble to find the resulting distribution of $S_i$. Averaging is carried out first over all parcels reaching a given cloud level with vertical velocity $u_j$ (referred to as the "$j$th cloud velocity state"), and then averaging over all cloud states. Based on this, the average saturation ratio, $S_\mathrm{o}$, of the cloud over a time interval $\Delta t$ is

$$S_\mathrm{o}(t) = \int_{-\infty}^{+\infty} \int_{X(t)} \int_{0}^{1} S_i(\mu, \tilde{x}, \tau) P(\mu, \tilde{x}, \tau) d\tau d\tilde{x} d\mu \tag{4}$$

where, $\mu = \frac{u}{\overline{u}}$, $u$ and $\overline{u}$ are the instantaneous and average vertical velocity, respectively, $\tilde{\mathbf{x}}$ is a vector (in dimensionless form) that denotes the position in the cloud, $\tau = \frac{t'}{\Delta t}$, where $t'$ is the averaging time, and $X(t)$ is the domain of $\tilde{x}$. $P(\mu, \tilde{x}, \tau)$ is the normalized probability at time $t'$ of finding a parcel between position $\tilde{x}$ and $\tilde{x} + d\tilde{x}$ (where $d\tilde{x} = \frac{dxdydz}{V_{\mathrm{cloud}}}$), with vertical velocity within $u$ and $u + du$.

Equation (4) can be simplified, by considering that fluctuations generated by gravity waves are random in nature (i.e., follow a Gaussian distribution, Fig. 4). Thus, under the assumption that does not vary with space and time within $\Delta t$, $P(\mu, \tilde{x}, \tau) = P(\mu)$ and



ACPD
10, 30857–30891, 2010

The two faces of cirrus clouds

D. Barahona and A. Nenes

Eq. (4) simplifies to

$$S_o(t) = \int_{-\infty}^{+\infty} \int_{X(t)} \int_0^1 S_i(\mu, \tilde{x}, \tau) P(\mu) d\tau d\tilde{x} d\mu \tag{5}$$

Equation (5) assumes that $S_o$ is affected by processes that act throughout the volume of the cirrus cloud. Other processes, like entrainment and radiative cooling, are neglected. Although this will not affect the conclusions of our study, they could be included in future studies indirectly through appropriate modification of the vertical velocity distribution (e.g., Barahona and Nenes, 2007).

Defining $\overline{S}_j = \int_{X(t)} \int_0^1 S_i(\mu, \tilde{x}, \tau) d\tau d\tilde{x}$ as the average supersaturation of parcels in the "$j$" velocity state over the time interval $\Delta t$, Eq. (5) can be rewritten as

$$S_o(t) = \int_{-\infty}^{+\infty} \overline{S}_j(\mu_j) P(\mu_j) d\mu_j \tag{6}$$

the time derivative of which gives,

$$\frac{dS_o}{dt} = \int_{-\infty}^{+\infty} \frac{d\overline{S}_j(\mu_j)}{dt} P(\mu_j) d\mu_j + \int_{-\infty}^{+\infty} \overline{S}_j(\mu_j) \frac{dP(\mu_j)}{dt} d\mu_j \tag{7}$$

the second integral on the right hand side of Eq. (7) depends on the source of vertical velocity fluctuations. Distant sources of gravity waves result in stationary $P(\mu_j)$, and $\frac{dP(\mu_j)}{dt} \rightarrow 0$. However $P(\mu_j)$ can be perturbed by near convective and orographic sources; in such cases $P(\mu_j)$ is not completely Gaussian and exhibits a tail towards high velocities (Bacmeister et al., 1999). For the purpose of this study it is assumed that $\frac{dP(\mu_j)}{dt} = 0$, which implies that the characteristic amplitude of temperature fluctuations, $\delta T$, remains constant during the entire period of simulation. Equation (7) then



ACPD
10, 30857–30891, 2010

becomes

$$\frac{dS_o}{dt} \approx \int_{-\infty}^{+\infty} \frac{d\overline{S}_j(\mu_j)}{dt} P(\mu_j) d\mu_j \tag{8}$$

Using the definition of $\overline{S}_j$,

$$\frac{d\overline{S}_j}{dt} = \int_{X(t)} \int_0^1 \frac{dS_i(\mu,\tilde{x},\tau)}{dt} d\tau d\tilde{x} \tag{9}$$

Substitution of Eq. (3) into above provides

$$\frac{d\overline{S}_j}{dt} = \int_{X(t)} \int_0^1 \left\{ \alpha u_j S_i - \frac{(S_i - 1)}{\tau_{\mathrm{rel},i}} \right\} d\tau d\tilde{x} = \alpha u_j \int_{X(t)} \int_0^1 S_i d\tau d\tilde{x} - \int_{X(t)} \int_0^1 \left( \frac{S_i - 1}{\tau_{\mathrm{rel},i}} \right) d\tau d\tilde{x} \tag{10}$$

which can be rewritten as,

$$\frac{d\overline{S}_j}{dt} = \alpha u_j \overline{S}_j - \int_{X(t)} \int_0^1 \left( \frac{S_i - 1}{\tau_{\mathrm{rel},i}} \right) d\tau d\tilde{x} \tag{11}$$

Introducing $\overline{S}_{\mathrm{eff},j}$ so that,

$$\int_{X(t)} \int_0^1 \left( \frac{S_i - 1}{\tau_{\mathrm{rel},i}} \right) d\tau d\tilde{x} = \left( \overline{S}_{\mathrm{eff},j} - 1 \right) \int_{X(t)} \int_0^1 \frac{1}{\tau_{\mathrm{rel},i}} d\tau d\tilde{x} \tag{12}$$

From Eq. (3),

$$\frac{1}{\tau_{\mathrm{rel},j}} = \int_{X(t)} \int_0^1 \frac{1}{\tau_{\mathrm{rel},i}} d\tau d\tilde{x} = \left[ \beta N_c \overline{D}_c \right]_{\mu=\mu_j} \tag{13}$$



ACPD
10, 30857–30891, 2010

The two faces of cirrus clouds

D. Barahona and A. Nenes

Combining Eqs. (12) and (13), Eq. (11) can be written as

$$\frac{d\overline{S}_j}{dt} = \alpha u_j \overline{S}_j - \frac{\overline{S}_{\text{eff},j} - 1}{\tau_{\text{rel},j}} \tag{14}$$

where $\tau_{\text{rel},j}$ is the relaxation time scale associated with the $j$th state. $\overline{S}_{\text{eff},j}$ is an "effective" saturation ratio for deposition/sublimation processes, defined below. Introducing Eq. (14) into Eq. (8),

$$\frac{dS_\text{o}}{dt} = \int_{-\infty}^{+\infty} \left( \alpha u_j \overline{S}_j - \frac{\overline{S}_{\text{eff},j} - 1}{\tau_{\text{rel},j}} \right) P(\mu_j) d\mu_j \tag{15}$$

or,

$$\frac{dS_\text{o}}{dt} = \int_{-\infty}^{+\infty} \alpha u_j \overline{S}_j P(\mu_j) d\mu_j - \int_{-\infty}^{+\infty} \left( \frac{\overline{S}_{\text{eff},j} - 1}{\tau_{\text{rel},j}} \right) P(\mu_j) d\mu_j \tag{16}$$

The first term in the right hand side of Eq. (16) must be equal to $\overline{u} S_\text{o}$, as in the absence of deposition/sublimation, $S_\text{o}$ in the layer increases exponentially with time (Pruppacher and Klett, 1997). With this, Eq. (16) becomes,

$$\frac{dS_\text{o}}{dt} = \frac{S_\text{o}}{\tau_\text{lift}} - \int_{-\infty}^{+\infty} \left( \frac{\overline{S}_{\text{eff},j} - 1}{\tau_{\text{rel},j}} \right) P(\mu_j) d\mu_j \tag{17}$$

where $\tau_\text{lift} = \left(\alpha \overline{u}\right)^{-1}$. Equation (17) must be solved for each time step specifying $P(\mu_j)$ and then evaluating $\overline{S}_{\text{eff},j}$ and the integral on the right hand side. Since is determined by the random overlapping of gravity waves of different frequency and amplitude (e.g.,



ACPD
10, 30857–30891, 2010
The two faces of cirrus clouds
D. Barahona and A. Nenes

$u_j$ is given by a Fourier series in time, Sect. 3.3), then for a time step of integration much smaller than $\tau_{\text{lift}}$ ($\sim 10^2$ s) Eq. (17) can be approximated by

$$\frac{dS_o}{dt} = \alpha\bar{u}S_o - \sum_{-N/2}^{N/2} \frac{\bar{S}_{\text{eff},j} - 1}{\tau_{\text{rel},j}} \tag{18}$$

where $N \sim \frac{\tau_{\text{lift}}}{\Delta t_{\text{step}}}$, and $\Delta t_{\text{step}}$ is the time step of integration.

Equation (18) gives the evolution of the $S_o$ in the cirrus cloud; its solution however requires the knowledge of $\bar{S}_{\text{eff},j}$. This is accomplished by considering the properties of the different parcels reaching the cloud layer at $t$. For example, if $S_i$ in the $i$th parcel is a pseudo-steady state, $\frac{dS_i}{dt} \sim 0$ (Korolev and Mazin, 2003) and from Eq. (3),

$$S_{i,\text{ss}} = \frac{\tau_{\text{lift},i}}{\tau_{\text{lift},i} - \tau_{\text{rel},i}} \tag{19}$$

where $\tau_{\text{lift},i} = (\alpha u_i)^{-1}$ and $S_{i,\text{ss}}$ is the steady state saturation ratio in the $i$th parcel. If $\tau_{\text{lift},i}<0$ then $S_{i,\text{ss}}<1$, and vice-versa. Thus, if $u_j<0$, the layer would likely be subsaturated over $\Delta t$ (e.g., Eq. 6), and vice-versa when $u_j>0$. Thus, depending on the sign of $u_j$ there is net deposition/sublimation of water vapor in the cloud layer. Not all parcels however reach steady state; therefore the degree of saturation/subsaturation associated with the $j$th state depends on the probability distribution of saturation within the cloudy layer, $P_s(S,S_o,\delta T)$, which is a function of $S_o$ and the average amplitude of temperature fluctuations, $\delta T$. Thus, $S_{\text{eff}}$ for $u_j<0$ is found by averaging over all states that would lead to subsaturation, i.e., $P_s(S,\delta T,S_o)$ for which $S<1$. Similarly, when $u_j>0$, the supersaturated ($S>1$) region of $P_s(S,\delta T,S_o)$ is used,

$$\bar{S}_{\text{eff},j} = \frac{\int_a^b S\frac{dP_s(S,\delta T,S_o)}{dS}dS}{\int_a^b \frac{dP_s(S,\delta T,S_o)}{dS}dS} \quad \text{where } a = \begin{cases} 1 & u_j > 0 \\ 0 & u_j \le 0 \end{cases} \quad \text{and } b = \begin{cases} S_{\text{hom}} & u_j > 0 \\ 1 & u_j \le 0 \end{cases} \tag{20}$$

The homogeneous freezing threshold, $S_{hom}$, is set as the upper limit of $P_s(\delta T, S_o)$ as ice crystal production quickly removes supersaturation above $S_{hom}$ (Kärcher and Burkhardt, 2008; Kärcher and Haag, 2004).

### 3.2 Evolution of ice crystal number concentration

The evolution of the number concentration within a cloudy layer is given by

$$\frac{dN_c}{dt} = \left.\frac{dN_c}{dt}\right|_{fr} + \left.\frac{dN_c}{dt}\right|_{sed} \tag{21}$$

where $\frac{dN_c}{dt}|_{fr}$ is the rate production of ice crystals within the layer, and $\frac{dN_c}{dt}|_{sed}$ is their sedimentation rate. Ice crystal freezing is a local process and occurs within single parcels when $S_i > S_{hom}$ and $u_i > 0$. The maximum ice crystal concentration frozen within the $i$th parcel is given by (Barahona and Nenes, 2008; Pruppacher and Klett, 1997)

$$N_{c,i} = N_o \left\{ 1 - \exp\left( - \int_0^{t_{max,i}} \overline{v}_o J(S_i) dt \right) \right\} \tag{22}$$

where $t_{max,i}$ is the time at which crystal freezing stops, $J$ is the homogeneous nucleation rate coefficient and $N_o$, $\overline{v}_o$ are the deliquesced aerosol number concentration and average volume, respectively. Taking the time derivative of Eq. (22) gives,

$$\left.\frac{dN_{c,i}}{dt}\right|_{fr} = N_o \overline{v}_o J(S_i) \exp\left( - \int_0^{t_{max,i}} \overline{v}_o J(S_i) dt \right) \tag{23}$$

which can be approximated by (Barahona and Nenes, 2008)

$$\left.\frac{dN_{c,i}}{dt}\right|_{fr} \approx N_o \overline{v}_o J_{max,i} \exp\left( - \frac{\overline{v}_o}{\alpha u_i} \int_0^{S_{max}} J(S_i) dS_i \right) \tag{24}$$



ACPD
10, 30857–30891, 2010
The two faces of cirrus clouds
D. Barahona and A. Nenes

where $J_{\max,i} = J(S_{\max,i})$. $S_{\max,i}$ is the maximum saturation ratio reached in the $i$th parcel, calculated by setting $\frac{dS_i}{dt} = 0$ in Eq. (1),

$$S_{\max,i} = \frac{\gamma}{\alpha u_i} \int_{\overline{D}_\mathrm{o}}^{\infty} D_{\mathrm{c},i}^2 \frac{dD_{\mathrm{c},i}}{dt} n_{i,\mathrm{nuc}}(D_\mathrm{c}) dD_\mathrm{c} \tag{25}$$

where $n_{i,\mathrm{nuc}}(D_\mathrm{c})$ is the size distribution of the recently nucleated ice crystals, and, $\overline{D}_\mathrm{o}$ is the mean size of the deliquesced aerosol. Equation (25) assumes that only recently nucleated ice crystals are contained within the parcel. In reality, a fraction of preexisting crystals remain in nucleation zones (typically located near the cloud top, Spichtinger and Gierens, 2009b) inhibiting the homogeneous freezing of ice. Ice crystals experience gravitational settling, hence only those crystals with terminal velocity, $u_\mathrm{term}$, below $\overline{u}$ would be found at the cloud top. Adding the consumption of water vapor from preexisting crystals to the right hand side of Eq. (25) gives

$$S_{\max,i} = \frac{\gamma}{\alpha u_i} \left[ \int_{\overline{D}_\mathrm{o}}^{\infty} D_{\mathrm{c},i}^2 \frac{dD_{\mathrm{c},i}}{dt} n_{i,\mathrm{nuc}}(D_\mathrm{c}) dD_\mathrm{c} + \int_{D_\mathrm{min}}^{D_\mathrm{term}} D_\mathrm{c}^2 \frac{dD_\mathrm{c}}{dt} n_\mathrm{c}(D_\mathrm{c}) dD_\mathrm{c} \right] \tag{26}$$

where $n_\mathrm{c}(D_\mathrm{c})$ is the cloud ice crystal size distribution, $D_\mathrm{term}$ is the size of the crystal for which $u_\mathrm{term} = \overline{u}$, and $D_\mathrm{min}$ is the minimum size of the preexisting crystals in the cloud. Equation (26) can be combined with Eq. (2) to obtain

$$S_{\max,i} = \frac{\gamma}{\alpha u_i} \left[ \int_{\overline{D}_\mathrm{o}}^{\infty} D_{\mathrm{c},i}^2 \frac{dD_{\mathrm{c},i}}{dt} n_{i,\mathrm{nuc}}(D_\mathrm{c}, S_{\max,i}) dD_\mathrm{c} + G N_\mathrm{c} \overline{D}_\mathrm{c} f_\mathrm{ps} (S_{\max,i} - 1) \right] \tag{27}$$

where, $f_\mathrm{ps} = \frac{1}{N_\mathrm{c}\overline{D}_\mathrm{c}} \int_{D_\mathrm{min}}^{D_\mathrm{term}} D_\mathrm{c} n_\mathrm{c}(D_\mathrm{c}) dD_\mathrm{c}$, is the fraction of preexisting ice crystals remaining in nucleation zones. As ice crystals remaining in the cloud layer were produced





ACPD
10, 30857–30891, 2010



Title Page
Abstract | Introduction
Conclusions | References
Tables | Figures
◂◂ | ▸▸
◂ | ▸
Back | Close
Full Screen / Esc
Printer-friendly Version
Interactive Discussion

by preexisting freezing events, Eq. (27) provides a link between the history of different parcels and the nucleation of new crystals. The analytical solution of Eq. (27) is presented elsewhere (Barahona and Nenes, 2009a; Barahona et al., 2010b).

The rate of ice crystal production in cloud velocity state $j$th is given by the concentration of nucleated crystals over the freezing timescale,

$$\left.\frac{dN_{c,j}}{dt}\right|_{\mathrm{fr}} = \frac{P_{\mathrm{s}}(S > S_{\mathrm{hom}})N_{\mathrm{o}}}{\tau_{\mathrm{fr},j}} H_{\mathrm{v}}(u_j) \tag{28}$$

where $\tau_{\mathrm{fr},j}^{-1} = \overline{V}_{\mathrm{o}} J_{\max,j} \exp(-\frac{\overline{V}_{\mathrm{o}}}{\alpha u_j}\int_0^{S\max} J(S_j)dS_j)$. $H_{\mathrm{v}}(u_j)$ is the Heaviside function and is introduced to account for the fact that homogeneous nucleation is very unlikely in parcels with negative vertical velocity (i.e., updraft must be maintained for some time before $S_{\mathrm{hom}}$ is reached after which it is quickly depleted by crystal nucleation and growth, Barahona and Nenes, 2008; Kärcher and Lohmann, 2002). $P_{\mathrm{s}}(S>S_{\mathrm{hom}})$ represents the fraction of parcels for which $S>S_{\mathrm{hom}}$. Using the same averaging procedure as for the supersaturation equation, we obtain

$$\left.\frac{dN_{\mathrm{c}}}{dt}\right|_{\mathrm{fr}} = N_{\mathrm{o}} \sum_{-N/2}^{N/2} P_{\mathrm{s}}(S > S_{\mathrm{hom}}) \left.\frac{H_{\mathrm{v}}(\mu_j)}{\tau_{\mathrm{fr},j}}\right|_{\mu=\mu_j} \tag{29}$$

Sedimentation processes out of the cloud layer depend primarily on the bulk properties of the cloud, i.e., the mean ice crystal size distribution and number concentration (interaction of individual parcels with falling crystals within the layer is accounted for in Eq. 27). The ice crystal loss rate by sedimentation is then given by,

$$\left.\frac{dN_{\mathrm{c}}}{dt}\right|_{\mathrm{sed}} = \frac{1}{H}\int_{D_{\min}}^{\infty} u_{\mathrm{term}}(D_{\mathrm{c}})n(D_{\mathrm{c}})dD_{\mathrm{c}} \tag{30}$$



ACPD
10, 30857–30891, 2010

The two faces of cirrus clouds

D. Barahona and A. Nenes

where $H$ is the cloud layer thickness. As $u_{\mathrm{term}} \sim D_{\mathrm{c}}$ (Heymsfield and Iaquinta, 2000). Equation (30) can be further simplified to

$$\left.\frac{dN_{\mathrm{c}}}{dt}\right|_{\mathrm{sed}} = \frac{N_{\mathrm{c}}\overline{u}_{\mathrm{term}}}{H} = \frac{N_{\mathrm{c}}}{\tau_{\mathrm{sed}}} \tag{31}$$

where $\overline{u}_{\mathrm{term}} = u_{\mathrm{term}}(\overline{D}_{\mathrm{c}})$.

## 3.3 Numerical solution

### 3.3.1 Competition between homogeneous and heterogeneous freezing

Calculation of ice crystal number concentration, $N_{\mathrm{c}}$ in in-situ cirrus from combined homogeneous and heterogeneous freezing in Figs. 1 and 2 is done using an analytical parameterization developed for in situ formed cirrus clouds and freezing fractions below 0.6 (Barahona and Nenes, 2009a). When the calculated freezing fraction exceeds 0.6, a sigmoidal increase in $N_{\mathrm{c}}$ is assumed (Barahona et al., 2010a), in agreement with parcel model simulations and field observations (Barahona and Nenes, 2008; DeMott et al., 2003). For combined homogeneous and heterogeneous freezing, it was assumed that the IN freeze instantaneously at a supersaturation freezing threshold, $s_{\mathrm{het}}$, of 15%, typical of deposition mode IN (Abbatt et al., 2006) with a 0.1 µm diameter at freezing (Froyd et al., 2009). Glassy aerosol was assumed to have a total concentration of 50 $\mathrm{cm}^{-3}$ and a freezing fraction given by the nucleation spectrum of Murray et al. (2010).

### 3.3.2 Vertical velocity

A spectrum of vertical velocity fluctuations was generated by superimposition of gravity waves from different sources (Bacmeister et al., 1999; Jensen and Pfister, 2004) expressed in the form $u = \overline{u} + \sum_j A(\varpi_j)\cos(\varpi_j t + mH + \phi)$ where $m$ is the vertical wave number, $H$ is the cloud thickness, and $\varpi_j$, $A(\varpi_j)$, and $\phi$, are the wave frequency, phase,



ACPD
10, 30857–30891, 2010

The two faces of cirrus clouds

D. Barahona and A. Nenes

and amplitude, respectively. For each simulation a time series of $u$ was generated over the frequency interval $\varpi = [3.35 \times 10^{-7}, 9.44 \times 10^{-4}]$ Hz (Jensen and Pfister, 2004), using randomly generated $\phi$ and $m$. $A(\varpi_j)$ was calculated using a power spectrum scaling law of $-1.85$ for $\varpi_j > 1 \times 10^{-5}$ Hz and of $-0.25$ for $\varpi_j \leq 1 \times 10^{-5}$ Hz (Jensen and Pfister, 2004). This procedure resulted in a normal distribution of $u$ (Fig. 4d) centered around $\overline{u}$. The maximum amplitude was assumed to occur at $\varpi_j = 1 \times 10^{-3}$ Hz (Jensen and Pfister, 2004) as it reproduces the results of Gayet et al. (2004) (Fig. 5 green line) which give positive $u$ around $0.23\,\mathrm{m\,s^{-1}}$ for $\delta T = 1$ K (i.e., $A(1 \times 10^{-3}) \approx 2.1 \delta T$). Representative time series for $u(t)$ are presented in Fig. 5.

### 3.3.3 Ice crystal freezing

The freezing timescale, $\tau_{\mathrm{fr},j}$, was calculated using the parameterization of Barahona and Nenes (2008, 2009a, b). Precursor aerosol was assumed to be composed of ammonium sulfate, lognormally distributed with dry mean geometric diameter of 40 nm, geometric dispersion of 2.3, and number concentration of $100\,\mathrm{cm^{-3}}$ (Lawson et al., 2008). To account for possible compositional impacts on crystal growth kinetics, the water-vapor deposition coefficient was varied between 0.006 (Magee et al., 2006) and 1.0. Homogeneous freezing is described using the parameterization of Koop et al. (2000). The term $P_s(S > S_{\mathrm{hom}})$ in Eq. (28) is the probability of finding $S$ above $S_{\mathrm{hom}}$, and is introduced to account for the threshold behavior of homogeneous freezing (Kärcher and Burkhardt, 2008; Koop et al., 2000). The effect of preexisting ice crystals on freezing was accounted for by allowing a fraction of $N_{\mathrm{c}}$ to deplete water vapor and increase $\tau_{\mathrm{fr},j}$ (Barahona and Nenes, 2009a; Barahona et al., 2010b). The fraction of pre-existing crystals remaining in freezing zones was calculated as, $f_{\mathrm{ps}} = \frac{1}{N_{\mathrm{c}}} \int_{D_{\mathrm{min}}}^{D_{\mathrm{term}}} n(D_{\mathrm{c}}) d D_{\mathrm{c}}$ where $n(D_{\mathrm{c}})$ is the ice crystal size distribution, $D_{\mathrm{min}}$ is the minimum pre-existing crystal size, and $D_{\mathrm{term}}$ is the crystal size for which its terminal velocity, $u_{\mathrm{term}}$, is equal to the uplift velocity of the cirrus later, $\overline{u}$. $u_{\mathrm{term}}$ was calculated assuming ice crystals have columnar shape with maximum dimension equal to $\overline{D}_{\mathrm{c}}$ (Heymsfield and Iaquinta,



ACPD
10, 30857–30891, 2010

2000). Following Heymsfield and Platt (1984) it was assumed $n(D_c) = AD_c^{-3.15}$; the parameters $A$ and $D_{\min}$ were calculated from the moments of $n(D_c)$: $N_c = \int_{D_{\min}}^{\infty} n(D_c)dD_c$ and $\overline{D}_c = \frac{1}{N_c}\int_{D_{\min}}^{\infty} D_c n(D_c)dD_c$. The calculation of $\overline{D}_c$ is described below. Integration of equations of Eqs. (18) and (21) was accomplished using a fixed time step of 2 s. Initial values for $N_c = 0.01\,\mathrm{cm}^{-3}$ and $S_o = 1.0$ were set. Using different initial values affected the time required to establish dynamic equilibrium (by a few hours) but did otherwise not affect the simulations.

#### 3.3.4 Ice crystal sedimentation

The rate of ice crystal sedimentation over the cloud scale, $H$, was assumed proportional to the terminal velocity of the mean crystal size $\overline{D}_c$ (Eq. 30). Other removal processes (ice crystal sublimation and detrainment) are neglected; $H$ however was varied over a wide interval (100 to 5000 m) to account for the uncertainty associated with neglecting these processes. $\overline{D}_c$ was calculated so that the total water vapor in the layer was partitioned between ice and vapor phases, i.e., $\overline{D}_c = \left(\frac{6q_{\mathrm{ice}}}{\pi\rho_i N_c}\right)^{1/3}$ where $q_{\mathrm{ice}} = q_{\mathrm{tot}} - \frac{p^o S_o M_w}{RT}$, $\rho_i$ is the ice density (Pruppacher and Klett, 1997), $R$ is the universal gas constant, $M_w$ is the molecular mass of water, and $p^o$ is the saturation water vapor pressure over ice (Murphy and Koop, 2005); the minimum ice crystal size was set to 4 µm in agreement with theoretical studies and experimental observations (Barahona and Nenes, 2008; Durran et al., 2009; Krämer et al., 2009). Loss of total water content, $q_{\mathrm{tot}}$, from the cloudy layer is also accounted for by solution of $\frac{dq_{\mathrm{tot}}}{dt} = -\frac{\pi}{6}\rho_i \overline{D}_c^3 \frac{dN_c}{dt}\Big|_{\mathrm{sed}}$. Representative time profiles of $\overline{D}_c$ and $q_{\mathrm{tot}}$ are presented in Fig. 5. The timescale of relaxation at $u = u_j$, $\tau_{\mathrm{rel},j}$, was calculated using $N_c$ and $\overline{D}_c$ of the cloud layer (e.q., Eq. 13).



Discussion Paper | Discussion Paper | Discussion Paper | Discussion Paper |

ACPD

10, 30857–30891, 2010

The two faces of cirrus clouds

D. Barahona and A. Nenes

## 4 Cirrus in dynamical equilibrium

Figure 4 presents the evolution of a cirrus layer subject to gravity-wave fluctuations with an initial average temperature of 195 K and lifting at $\overline{u} = 1\,\mathrm{cm\,s^{-1}}$. For values of $\delta T > 1$ K, the cloud initially experiences a strong homogeneous nucleation pulse, so that $N_c$ initially increases steeply (Fig. 4a); the consumption of water vapor by crystal growth decreases $S_o$ (Fig. 4b) which prevents any new freezing events. $N_c$ slowly decreases from sedimentation loss; only after enough ice crystals sediment out of the cloud layer, $S_o$ increases (e.g., $\delta T = 1$ K, green lines) and new freezing events occur. For $\delta T > 1.4$ K (purple lines) this is possible even if the layer remains on average subsaturated ($S_o < 1$) because the probability distribution of $S$ is broad enough for a non-negligible probability with $S > S_{hom}$. This "pulse-decay" behavior is characterized by $\tau_{sed} \gg \tau_{rel}$ so ice crystals reside long enough in the cloud to relax supersaturation (Fig. 4c); this behavior is also consistent with the parcel model concept of cirrus (where high $N_c$ and low $S_o$ coexist within the parcel). The subsaturation levels (Fig. 4) achieved in this state are in agreement with in situ observations of relative humidity in dissipating clouds (Gao et al., 2004; Krämer et al., 2009).

The cirrus evolution is however quite different when $\delta T$ is small; the distribution of $S$ is narrow, and substantial ice production is only possible after supersaturation (i.e., $S_o$) builds up in the cloudy layer to allow a non-negligible probability where $S > S_{hom}$. Thus, freezing events producing large $N_c$ (associated with large $u$ fluctuations; Fig. 4d) are less frequent. Low $N_c$ allows the formation of large ice crystals (Fig. 5) which sediment out of the layer before substantially depleting supersaturation, leading to new freezing events. This "dynamic equilibrium" between ice production and loss is a previously unidentified microphysical regime of cirrus, characterized by $\tau_{sed} \sim \tau_{rel,j}$ (Fig. 4c); it maintains low $N_c$ and high $S_o$ in the cloudy layer (Fig. 4a, b) and is consistent with observations of low-temperature cirrus. Clouds in "dynamic equilibrium" also exhibit broad crystal size distribution, because large ice crystals coexist with freshly-formed (small) crystals in the cloud (Fig. 5).





ACPD
10, 30857–30891, 2010

When simulations (such as those of Fig. 4) are placed on a "state diagram" of $N_c$ vs. $S_o$, the two microphysical regimes described above clearly emerge. Examples are presented in Figs. 6 and 7 for a range of initial conditions (presented as stars on the plots) and a variety of $\delta T$ (lines of distinct color). Progression towards a "dynamic equilibrium" is favored when supersaturation replenishes quickly (i.e., at high $\tau_{sed}$) and high $\overline{u}$; vice-versa for "pulse-decay" behavior. Figures 6 and 7 also show that the "dynamic equilibrium" state occurs spontaneously when $\delta T$ goes below a characteristic transition value (which depends on $\overline{u}$ and $T$). It can also be reached after a cloud initially resides in a "pulse-decay" state, if $\delta T$ is close to the characteristic value ($\delta T \sim 1$ K in Fig. 6). Clouds in the "dynamic equilibrium" regime are also much less sensitive to the presence of IN and to slow water vapor deposition (e.g., Fig. 6c). When maximum $N_c$ and time-averaged $S_o$ are presented on the state diagram for all simulations considered, the conditions of $\delta T$ that separate "pulse-decay" and "dynamic equilibrium" regimes seem to be universal (Fig. 8).

## 5 Conclusions and implications

From the discussion above, cold cirrus clouds will reside in the "dynamic equilibrium" regime if $\delta T$ is below the characteristic threshold. High-amplitude, orographically-generated gravity waves are ubiquitous (Kim et al., 2003) but often lose intensity with altitude, weakening their contribution to the background spectrum of temperature fluctuations. Thus, $\delta T$ can decrease enough at high altitude for cirrus to transition from a "pulse-decay" to a "dynamic equilibrium" regime (Fig. 8). This would explain why low $N_c$ and high $S_o$ are observed at low temperatures near the tropopause. Dynamical equilibrium is also possible at warmer conditions (particularly for high $\overline{u}$; Fig. 6d) but require small $\delta T$; given that high amplitude fluctuations are widespread at lower altitudes (Hoyle et al., 2005), cirrus clouds are likely forced to always follow a pulse-decaying behavior.





ACPD
10, 30857–30891, 2010

In summary, cirrus clouds at low temperature exhibit characteristics (e.g., low $N_c$ and high saturation ratios) that cannot be explained with the simple "conventional" picture of homogeneous freezing driven by expansion cooling. The prevailing hypothesis of heterogeneous freezing requires that only weak vertical movement (neglecting the presence of temperature fluctuations) force the formation of cirrus clouds in the upper troposphere, and therefore cannot alone explain the observed cirrus features. We show that small-scale fluctuations from the action of gravity waves can switch a cloud into a previously unknown "dynamic equilibrium" regime, with sustained levels of low $N_c$ and high saturation ratios consistent with "puzzling" characteristics observed in low temperature cirrus. With this study, a new understanding for cirrus clouds emerges, where the "unperturbed" microphysical state is one of dynamical equilibrium with low crystal number and high supersaturation. Only when the mean amplitude of temperature fluctuations exceeds a threshold value ($\delta T > 1$ K at cold temperatures), cirrus exhibit the well-known "pulse-decay" microphysical state. Throughout much of the atmosphere, the latter state dominates, simply because $\delta T$ is larger than the characteristic threshold value. In the TTL, $\delta T$ is still remarkably large (0.6–0.8 K) (Bacmeister et al., 1999; Jensen and Pfister, 2004; Sato, 1990), but does not systematically exceed the threshold for "pulse-decay" behavior, so cirrus regress to their "unperturbed" dynamic-equilibrium state.

The structure and responses of cirrus to dynamical and microphysical forcings can also be portrayed. For example, cirrus formed in the region of convective anvils might exhibit "pulse-decay" state until gravity-wave fluctuations decay to below the $\delta T$ threshold and transition to a dynamic-equilibrium state. For the same reasons, IN impacts on cirrus properties can be strong for clouds in pulse-decay state, but not for clouds in dynamic equilibrium. In conclusion, the discovery of dynamic equilibrium states reshapes our understanding of cirrus clouds and their role in anthropogenic climate change, as the type of dynamical forcing will set these clouds in one of two "preferred" microphysical regimes with very different susceptibility to anthropogenic aerosol.





ACPD
10, 30857–30891, 2010

*Acknowledgement.* This study was supported by NASA ACMAP and a NSF CAREER award.

## References

Abbatt, J. P. D., Benz, S., Cziczo, D. J., Kanji, Z., and Möhler, O.: Solid ammonium sulfate as ice nuclei: a pathway for cirrus cloud formation, Science, 313, 1770–1773, 2006.

Bacmeister, J., Eckermann, S. D., Tsias, A., Carslaw, K. S., and Peter, T.: Mesoscale temperature fluctuations induced by a spectrum of gravity waves: a comparison of parameterizations and their impact on stratospheric microphysics, J. Atmos. Sci., 56, 1913–1924, 1999.

Barahona, D. and Nenes, A.: Parameterization of cloud droplet formation in large scale models: including effects of entrainment, J. Geophys. Res., 112, D16026, doi:16010.11029/16207JD008473, 2007.

Barahona, D. and Nenes, A.: Parameterization of cirrus formation in large scale models: homogeneous nucleation, J. Geophys. Res., 113, D11211, doi:11210.11029/12007JD009355, 2008.

Barahona, D. and Nenes, A.: Parameterizing the competition between homogeneous and heterogeneous freezing in cirrus cloud formation – monodisperse ice nuclei, Atmos. Chem. Phys., 9, 369–381, doi:10.5194/acp-9-369-2009, 2009a.

Barahona, D. and Nenes, A.: Parameterizing the competition between homogeneous and heterogeneous freezing in ice cloud formation – polydisperse ice nuclei, Atmos. Chem. Phys., 9, 5933–5948, doi:10.5194/acp-9-5933-2009, 2009b.

Barahona, D., Rodriguez, J., and Nenes, A.: Sensitivity of the global distribution of cirrus ice crystal concentration to heterogeneous freezing, J. Geophys. Res., 115, D23213, doi:10.1029/2010JD014273, 2010.

Barahona, D., West, R. E. L., Stier, P., Romakkaniemi, S., Kokkola, H., and Nenes, A.: Comprehensively accounting for the effect of giant CCN in cloud activation parameterizations, Atmos. Chem. Phys., 10, 2467–2473, doi:10.5194/acp-10-2467-2010, 2010b.

DeMott, P. J., Cziczo, D. J., Prenni, A. J., Murphy, D. M., Kreidenweis, S. M., Thompson, D. S., Borys, R., and Rogers, D. C.: Measurements of the concentration and composition of nuclei for cirrus formation, P. Natl. Acad. Sci. USA, 100, 14655–14660, 2003.

Durran, D. R., Dinh, T., Ammerman, M., and Ackerman, T.: The mesoscale dynamics of

thin tropical tropopause cirrus, J. Atmos. Sci., 66, 2859–2873, doi:10.1175/2009JAS3046.1, 2009.
Fountoukis, C. and Nenes, A.: ISORROPIA II: a computationally efficient thermodynamic equilibrium model for $K^+$–$Ca^{2+}$–$Mg^{2+}$–$NH^{4+}$–Na+–$SO_4{}^{2-}$–$NO_3{}^-$–$Cl^-$–$H_2O$ aerosols, Atmos. Chem. Phys., 7, 4639–4659, doi:10.5194/acp-7-4639-2007, 2007.
Fridlind, A. M., Ackerman, A. S., Jensen, E. J., Heymsfield, A. J., Poellot, M. R., Stevens, D. E., Wang, D., Miloshevich, L. M., Baumgardner, D. G., Lawson, P., Willson, J., Flagan, R. C., Seinfeld, J. H., Jonsson, H. H., VanReken, T. M., Varutbangkul, V., and Rissman, T. A.: Evidence for the predominance of mid-tropospheric aerosols as subtropical anvil cloud nuclei, Science, 304, 718–722, 2004.
Froyd, K. D., Murphy, D. M., Sanford, T. J., Thomson, D. S., Wilson, J. C., Pfister, L., and Lait, L.: Aerosol composition of the tropical upper troposphere, Atmos. Chem. Phys., 9, 4363–4385, doi:10.5194/acp-9-4363-2009, 2009.
Gao, R. S., Popp, P. J., Fahey, D. W., Marcy, T. P., Herman, R. L., Weinstock, E. M., Baumgardner, D. G., Garrett, T. J., Rosenlof, K. H., Thompson, T. L., Bui, P. T., Ridley, B. A., Wofsy, S. C., Toon, O. B., Tolbert, M. A., Kärcher, B., Peter, T., Hudson, P. K., Weinheimer, A. J., and Heymsfield, A. J.: Evidence that nitric acid increases relative humidity in low-temperature cirrus clouds, Science, 303, 516–520, 2004.
Gayet, J. F., Ovarlez, J., Shcherbakov, V., Ström, J., Schumann, U., Minikin, A., Auriol, F., Petzold, A., and Monier, M.: Cirrus cloud microphysical and optical properties at southern and northern midlatitudes during the INCA experiment, J. Geophys. Res., 109, D20206, doi:20210.21029/22004JD004803, 2004.
Herzog, A. and Vial, F.: A study of the dynamics of the equatorial lower stratosphere by use of ultra-long-duration balloons, J. Geophys. Res., 106, 22745–22761, 2001.
Heymsfield, A. J. and Iaquinta, J.: Cirrus crystals terminal velocities, J. Atmos. Sci., 57, 916–938, 2000.
Heymsfield, A. J. and Platt, C. M.: A parameterization of the particle size spectrum of ice clouds in terms of the ambient temperature and ice water content, J. Atmos. Sci., 41, 846–855, 1984.
Heymsfield, A. J. and Sabin, R. M.: Cirrus crystal nucleation by homogenous freezing of solution droplets, J. Atmos. Sci., 46, 2252–2264, 1989.
Hoyle, C. R., Luo, B. P., and Peter, T.: The origin of high ice crystal number densities in cirrus clouds, J. Atmos. Sci., 62, 2658–2579, 2005.

Jensen, E. J. and Pfister, L.: Transport and freeze-drying in the tropical tropopause layer, J. Geophys. Res., 109, D02207, doi:02210.01029/02003JD004022, 2004.
Jensen, E. J., Smith, J. B., Pfister, L., Pittman, J. V., Weinstock, E. M., Sayres, D. S., Herman, R. L., Troy, R. F., Rosenlof, K., Thompson, T. L., Fridlind, A. M., Hudson, P. K., Cziczo, D. J., Heymsfield, A. J., Schmitt, C., and Wilson, J. C.: Ice supersaturations exceeding 100% at the cold tropical tropopause: implications for cirrus formation and dehydration, Atmos. Chem. Phys., 5, 851–862, doi:10.5194/acp-5-851-2005, 2005.
Jensen, E. J., Pfister, L., Bui, T. V., Lawson, P., Baker, B., Mo, Q., Baumgardner, D., Weinstock, E. M., Smith, J. B., Moyer, E. J., Hanisco, T. F., Sayres, D. S., Clair, J. M. S., Alexander, M. J., Toon, O. B., and Smith, J. A.: Formation of large (∼100 µm) ice crystals near the tropical tropopause, Atmos. Chem. Phys., 8, 1621–1633, doi:10.5194/acp-8-1621-2008, 2008.
Jensen, E. J., Pfister, L., Bui, T.-P., Lawson, P., and Baumgardner, D.: Ice nucleation and cloud microphysical properties in tropical tropopause layer cirrus, Atmos. Chem. Phys., 10, 1369–1384, doi:10.5194/acp-10-1369-2010, 2010.
Kärcher, B. and Burkhardt, U.: A cirrus scheme for global circulation models, Q. J. R. Meteorol. Soc., 134, 1439–1461; doi:1410.1002/Qj.1301, 2008.
Kärcher, B. and Haag, W.: Factors controlling upper tropospheric relative humidity, Ann. Geophys., 22, 705–715, doi:10.5194/angeo-22-705-2004, 2004.
Kärcher, B. and Lohmann, U.: A parameterization of cirrus cloud formation: homogeneous freezing of supercooled aerosols, J. Geophys. Res., 107, 4010, doi:4010.1029/2001JD000470, 2002.
Kay, J. E., Baker, M., and Hegg, D.: Physical controls on orographic cirrus inhomogeneity, Atmos. Chem. Phys., 7, 3771–3781, doi:10.5194/acp-7-3771-2007, 2007.
Kim, Y.-J., Eckermann, S. D., and Chun, H.-Y.: An overview of the past, present, and future of gravity-wave drag parameterization for numerical climate and weather prediction models, Atmos. Ocean, 41, 65–98, 2003.
Koop, T., Luo, B., Tslas, A., and Peter, T.: Water activity as the determinant for homogeneous ice nucleation in aqueous solutions, Nature, 406, 611–614, 2000.
Korolev, A. V. and Mazin, I. P.: Supersaturation of water vapor in clouds, J. Atmos. Sci., 60, 2957–2974, 2003.
Krämer, M., Schiller, C., Afchine, A., Bauer, R., Gensch, I., Mangold, A., Schlicht, S., Spelten, N., Sitnikov, N., Borrmann, S., de Reus, M., and Spichtinger, P.: Ice supersaturations

and cirrus cloud crystal numbers, Atmos. Chem. Phys., 9, 3505–3522, doi:10.5194/acp-9-3505-2009, 2009.
Lawson, R. P., Pilson, B., Baker, B., Mo, Q., Jensen, E., Pfister, L., and Bui, P.: Aircraft measurements of microphysical properties of subvisible cirrus in the tropical tropopause layer, Atmos. Chem. Phys., 8, 1609–1620, doi:10.5194/acp-8-1609-2008, 2008.
Liou, K.: Influence of cirrus clouds on weather and climate processes: a global perspective, Mon. Weather Rev., 114, 1167–1199, 1986.
Lohmann, U. and Feichter, J.: Global indirect aerosol effects: a review, Atmos. Chem. Phys., 5, 715–737, doi:10.5194/acp-5-715-2005, 2005.
Magee, N., Moyle, A. M., and Lamb, D.: Experimental determination of the deposition coefficient of small cirrus-like ice crystals near −50°C, Geophys. Res. Lett., 33, L17813, doi:17810.11029/12006GL026665, 2006.
Murphy, D. M. and Koop, T.: Review of the vapour pressures of ice and supercooled water for atmospheric applications, Q. J. R. Meteorol. Soc., 131, 1539–1565, 2005.
Murray, B. J.: Inhibition of ice crystallisation in highly viscous aqueous organic acid droplets, Atmos. Chem. Phys., 8, 5423–5433, doi:10.5194/acp-8-5423-2008, 2008.
Murray, B. J., Knopf, D. A., and Bertram, A. K.: The formation of cubic ice under conditions relevant to Earth's atmosphere, Nature, 434, 202–205, 2005.
Murray, B. J., Wilson, T. W., Dobbie, S., Cui, Z., Al-Jumur, S. M. R. K., Möhler, O., Schnaiter, M., Wagner, R., Benz, S., Niemand, M., Saathoff, H., Ebert, V., Wagner, S., and Kärcher, B.: Heterogeneous nucleation of ice particles on glassy aerosol under cirrus conditions, Nature Geosci., 3, 233–237, 2010.
Peter, T.: Microphysics and heterogeneous chemistry of polar stratospheric clouds, Annu. Rev. Phys. Chem., 48, 785–822, 1997.
Peter, T., Marcolli, C., Spichtinger, P., Corti, T., Baker, B., and Koop, T.: When dry air is too humid, Science, 314, 1399–1401, 2006.
Pruppacher, H. R. and Klett, J. D.: Microphysics of Clouds and Precipitation, 2nd edn., Kluwer Academic Publishers, Boston, MA, 954 pp., 1997.
Ramanathan, V. and Collins, W.: Thermodynamic regulation of ocean warming by cirrus clouds deduced from observations of 1987 El Nino, Nature, 351, 27–32, 1991.
Sato, K.: Vertical wind disturbances in the troposphere and lower stratosphere observed by the MU radar, J. Atmos. Sci., 47, 2803–2817, 1990.
Seinfeld, J. H.: Clouds, contrails and climate, Nature, 391, 837–838, 1998.





ACPD
10, 30857–30891, 2010

The two faces of cirrus clouds

D. Barahona and A. Nenes

Seinfeld, J. H. and Pandis, S. N.: Atmospheric Chemistry and Physics, John Wiley and Sons, New York, NY, USA, 1998.
Shilling, J. E., Fortin, T. J., and Tolbert, M. A.: Depositional ice nucleation on crystalline organic and inorganic solids, J. Geophys. Res., 111, D12204, doi:12101.11029/12005JD006664, 2006.
Spichtinger, P. and Gierens, K. M.: Modelling of cirrus clouds – Part 2: Competition of different nucleation mechanisms, Atmos. Chem. Phys., 9, 2319–2334, doi:10.5194/acp-9-2319-2009, 2009a.
Spichtinger, P. and Gierens, K. M.: Modelling of cirrus clouds – Part 1b: Structuring cirrus clouds by dynamics, Atmos. Chem. Phys., 9, 707–719, doi:10.5194/acp-9-707-2009, 2009b.
Wise, M. E., Baustian, K. J., and Tolbert, M. A.: Internally mixed sulfate and organic particles as potential ice nuclei in the tropical tropopause region, P. Natl. Acad. Sci. USA, 107, 15, 6693–6698, doi:6610.1073/pnas.0913018107, 2010.





ACPD
10, 30857–30891, 2010

The two faces of cirrus clouds

D. Barahona and A. Nenes

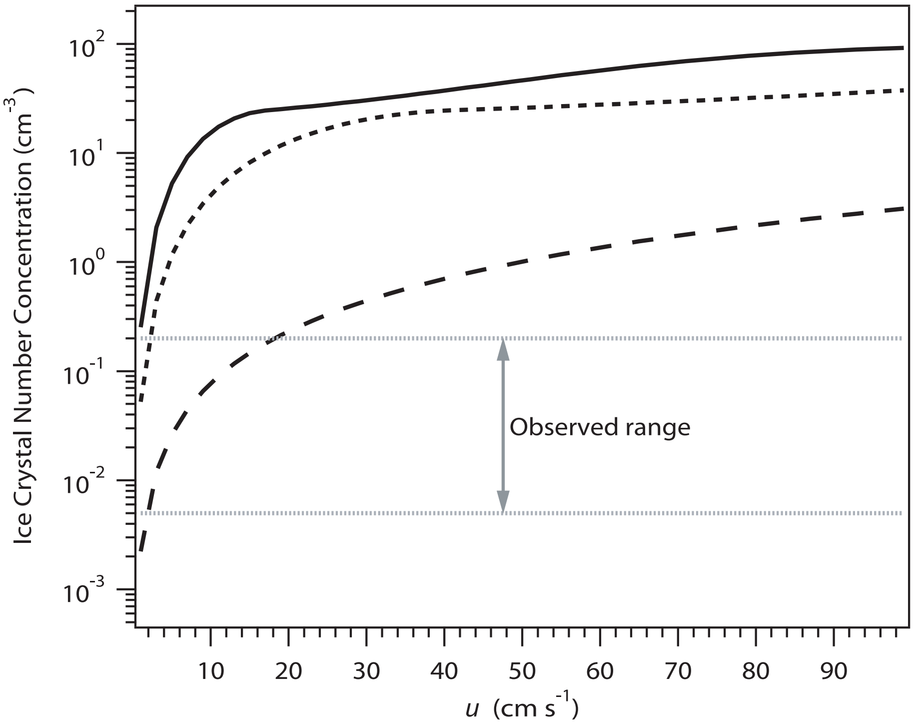


**Fig. 1.** Ice crystal concentration, $N_c$, as a function of updraft velocity, $u$. Cloud was assumed to form at $T = 185$ K and $p = 100$ hPa (details provided in the METHODS section). Low values of $u$ correspond to cloud formation driven primarily by large scale dynamics, whereas $u > 50$ cm s$^{-1}$ is characteristic of cirrus developing in the vicinity of convective systems with intense gravity wave breaking (Kim et al., 2003). Solid lines indicate $N_c$ calculated for pure homogeneous freezing, dashed lines for $N_{IN} = N_{lim}$, and dotted for $N_{IN} = 0.75N_{lim}$. For $N_{IN} = N_{lim}$, $N_c$ lies close to the observed values for $u < 50$ cm s$^{-1}$ (Krämer et al., 2009) but is very sensitive to small fluctuations in $N_{IN}$.





ACPD
10, 30857–30891, 2010

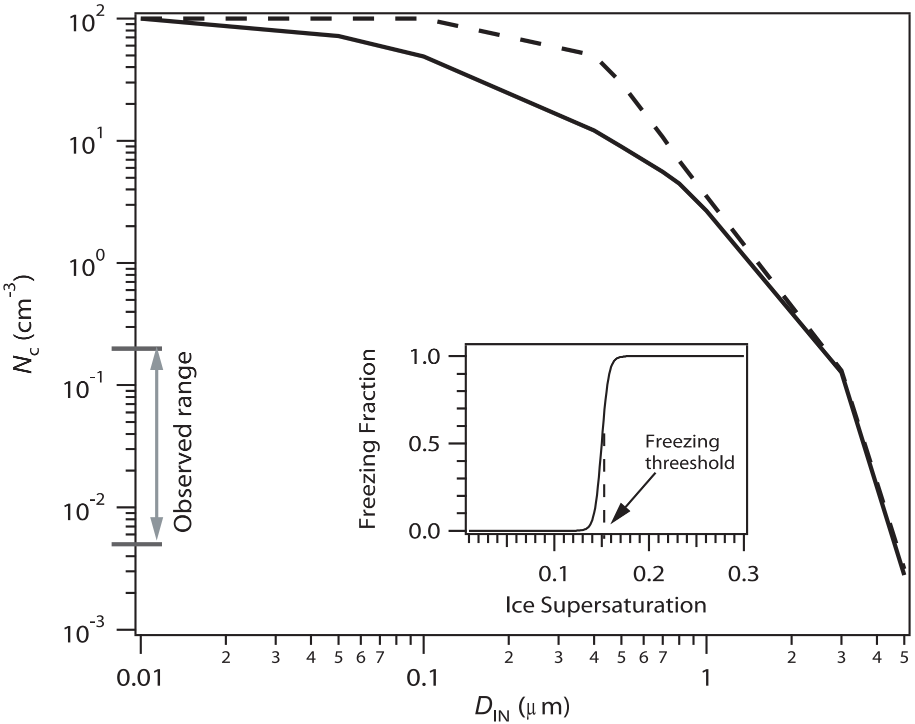


**Fig. 2.** Simulations of ice crystal concentration by pure heterogeneous freezing using the "conventional" model of cirrus formation (i.e., fluctuations in $S$ and $u$ from fluctuations in temperature are neglected). $N_c$ is presented as a function of the initial size of the ice nuclei. Conditions (Lawson et al., 2008) used were $T$ =185 K, $p$=100 hPa, $\alpha_d$ = 0.07 (dashed line), and 1.0 (solid line). The IN population was assumed to be monodisperse with total number concentration of 100 cm$^{-3}$ (Lawson et al., 2008). Consistent with published studies (Abbatt et al., 2006), freezing of solid ammonium sulfate was assumed to occur in a "burst" around the heterogeneous freezing threshold described by sigmoidal freezing spectrum with inflection point , where 99% of the aerosol freeze within a 2% supersaturation interval about (inset plot).





ACPD
10, 30857–30891, 2010

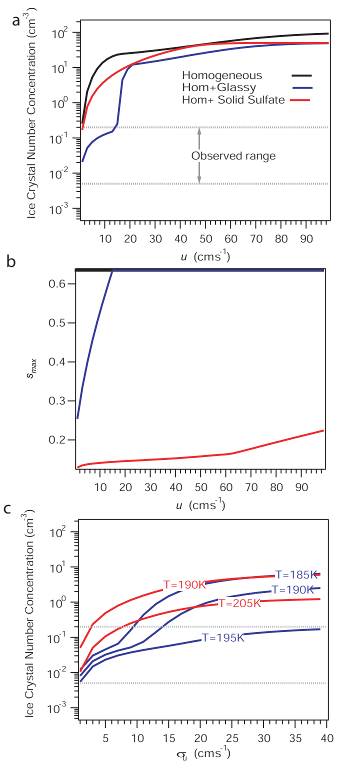


**Fig. 3.** Comparison between heterogeneous effects from solid ammonium sulfate (Abbatt et al., 2006) and glassy citric acid aerosol (Murray et al., 2010), using the analytical model of Barahona and Nenes (2009b) for homogeneous and heterogeneous freezing. **(a)** Maximum ice crystal concentration as a function of updraft velocity for a single freezing event. **(b)** Maximum supersaturation achieved for a single freezing event. **(c)** Ice crystal concentration averaged over a normal distribution of updraft velocities with zero mean and standard deviation $\sigma_u$. The gray lines represent the range of $N_c$ typically observed (Krämer et al., 2009).





ACPD
10, 30857–30891, 2010

The two faces of cirrus clouds

D. Barahona and A. Nenes

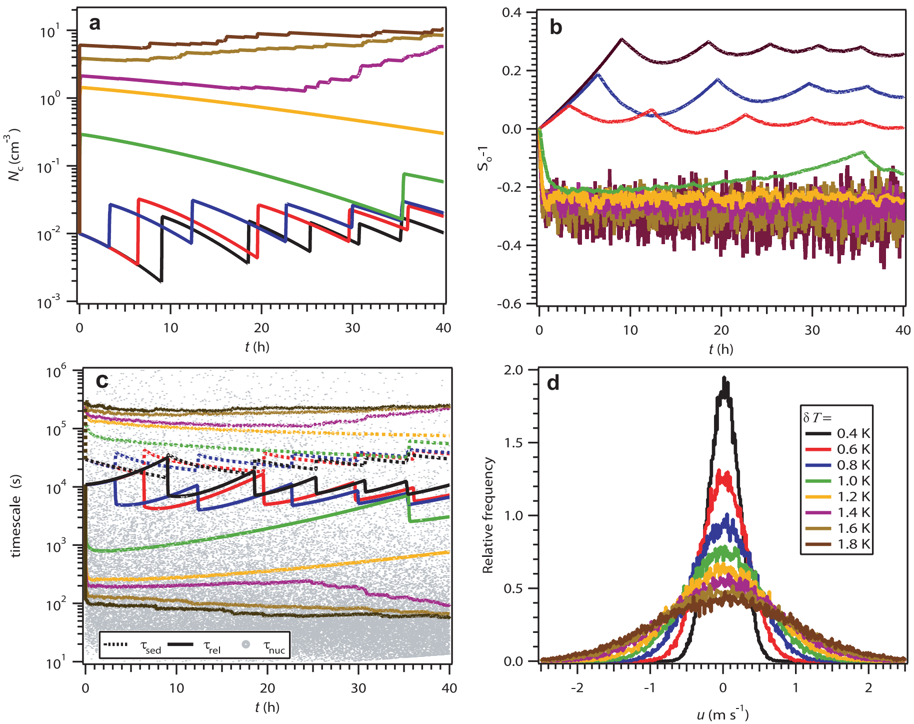


**Fig. 4.** Evolution of a cirrus cloud lifting at $1\,\mathrm{cm\,s^{-1}}$ with initial $T = 195\,\mathrm{K}$ and cloud thickness, $H = 500\,\mathrm{m}$, and using a water vapor to ice deposition coefficient equal to 1. Shown are **(a)** the ice crystal number concentration, **(b)** mean supersaturation, **(c)** characteristic timescales of freezing (gray dots), relaxation (solid lines), and sedimentation (dotted lines), and, **(d)** frequency distribution of vertical velocity, for different values of the mean amplitude temperature fluctuations, $\delta T$. For large fluctuations ($\delta T > 1\,\mathrm{K}$) most ice crystals form during the initial stage of cloud formation and the cloud slowly decays over time. For smaller fluctuations ($\delta T < 1\,\mathrm{K}$) a dynamic equilibrium states establishes where ice losses by sedimentation is compensated by production of new ice crystals, maintaining low $N_c$ and high $S_o$ over time.



ACPD

10, 30857–30891, 2010

**The two faces of cirrus clouds**

D. Barahona and A. Nenes

Title Page
Abstract | Introduction
Conclusions | References
Tables | Figures
◂◂ | ▸▸
◂ | ▸
Back | Close
Full Screen / Esc
Printer-friendly Version
Interactive Discussion

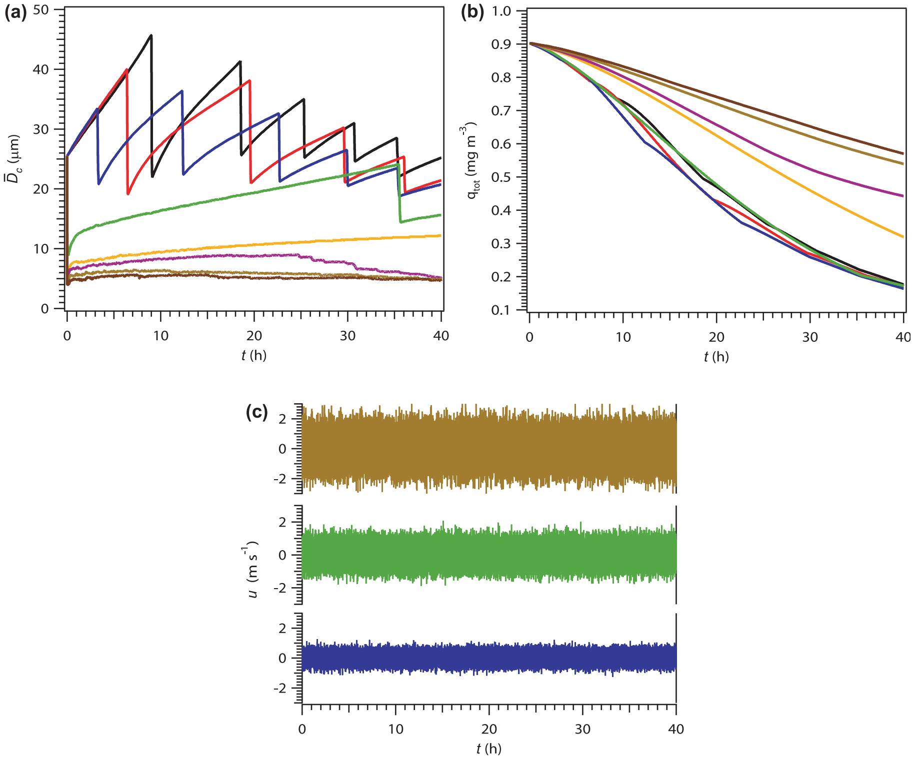


**Fig. 5.** Time series of mean ice crystal diameter, $\overline{D}_c$, total water content, $q_{tot}$, and updraft velocity, $u$, for the conditions presented in Fig. 4.



ACPD
10, 30857–30891, 2010
The two faces of cirrus clouds
D. Barahona and A. Nenes

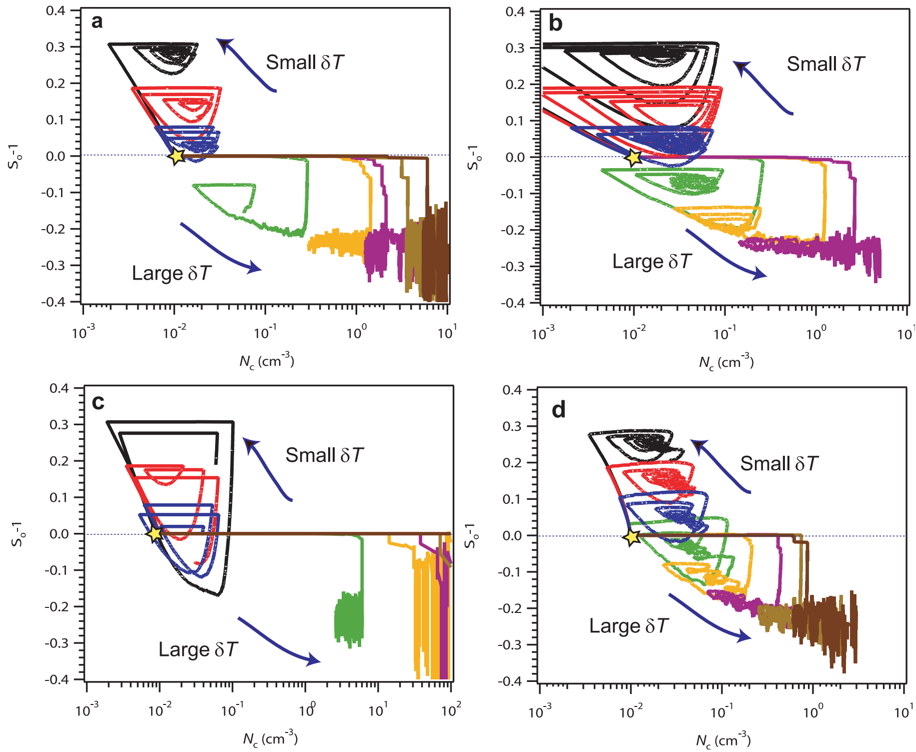


**Fig. 6.** Sensitivity of $N_c$ and $S_o$ evolution to cloud formation conditions for different values of $\delta T$ (color scheme same as in Fig. 4); **(a)** same conditions as in Fig. 4, **(b)** cloud thickness, $H = 100$ m (increased ice crystal removal rate), **(c)** deposition coefficient equal to 0.006 (Magee et al., 2006) (slow water vapor transfer), and **(d)** initial temperature 225 K and cloud lifting at 5 cm s$^{-1}$. The yellow star in each panel indicates initial conditions. The integration time was 40 h cases, except in **(d)** were it was 15 h.





ACPD
10, 30857–30891, 2010

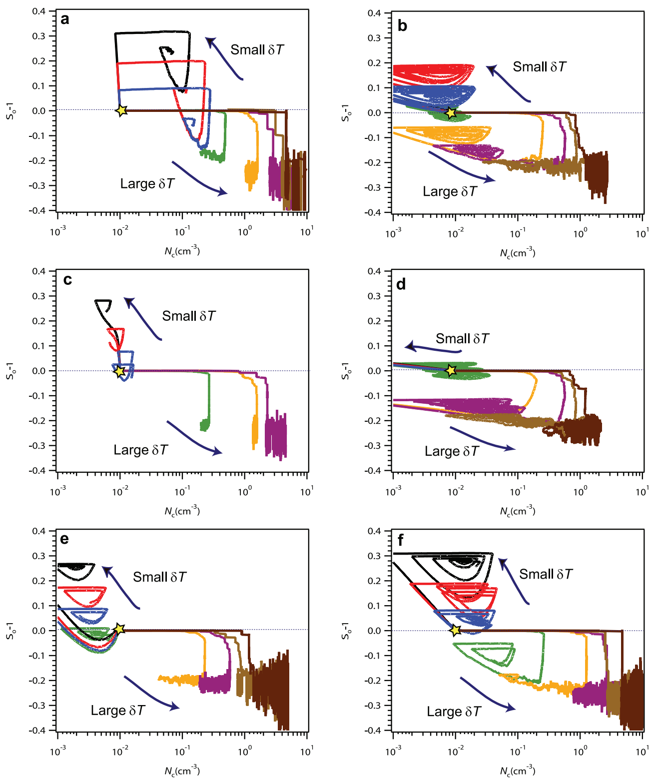


**Fig. 7.** Similar to Fig. 6, but varying cloud mean vertical velocity, $\overline{u}$, initial layer temperature, $T_o$, cloud thickness, $H$, and mean ice crystal terminal velocity, $u_{term}$. **(a)** $\overline{u} = 5\,\mathrm{cm\,s^{-1}}$, $H = 500\,\mathrm{m}$, $T_o = 195\,\mathrm{K}$; **(b)** $\overline{u} = 1\,\mathrm{cm\,s^{-1}}$, $H = 500\,\mathrm{m}$, $T_o = 225\,\mathrm{K}$; **(c)** $\overline{u} = 1\,\mathrm{cm\,s^{-1}}$, $H = 5000\,\mathrm{m}$, $T_o$=195 K; **(d)** $\overline{u} = 1\,\mathrm{cm\,s^{-1}}$, $H = 100\,\mathrm{m}$, $T_o = 225\,\mathrm{K}$; **(e)** $\overline{u} = 1\,\mathrm{cm\,s^{-1}}$, $H = 5000\,\mathrm{m}$, $T_o = 225\,\mathrm{K}$; **(f)** $\overline{u} = 1\,\mathrm{cm\,s^{-1}}$, $H$=500 m, $T_o = 195\,\mathrm{K}$, and $u_{term}$ multiplied by 2. The yellow star in each plot indicates initial conditions. The integration time was 40 h in for $\overline{u} = 1\,\mathrm{cm\,s^{-1}}$ and 15 h for $\overline{u} = 5\,\mathrm{cm\,s^{-1}}$.





ACPD
10, 30857–30891, 2010

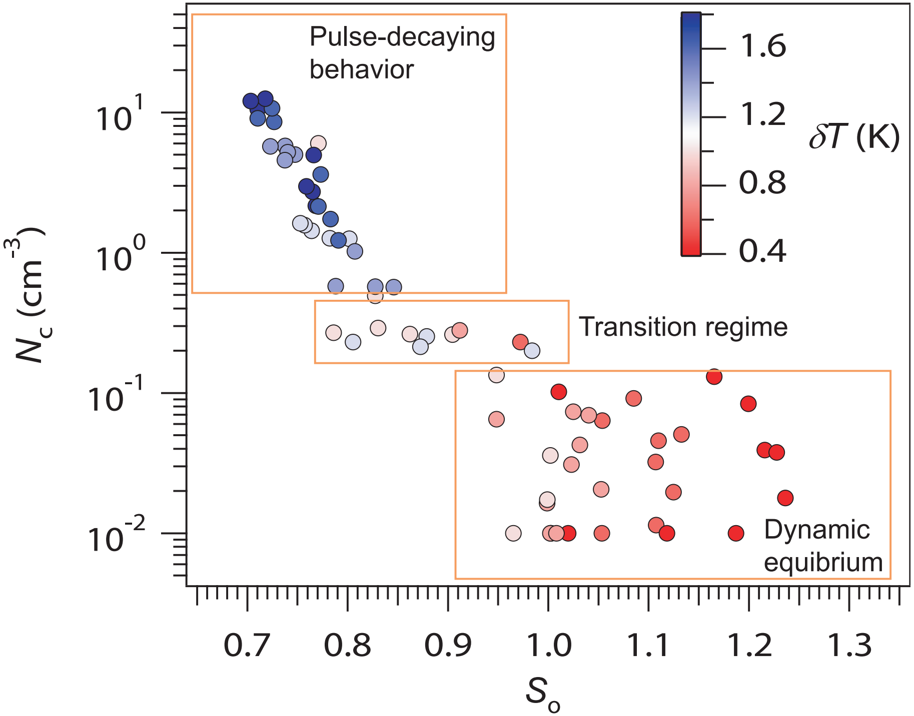


**Fig. 8.** Maximum ice crystal concentration obtained during the cloud evolution simulations against the time-averaged mean saturation ratio. Results presented for all simulations carried out in this study. Integration time varied between 15 and 40 h. Symbols are colored by the value of $\delta T$ used. Regions where the cloud spontaneously transitions to a "pulse-decay" and "dynamic equilibrium" state are noted; the "transitional" region marks where the cloud generally initially exhibited "pulse-decay" behavior over few hours and then transitioned to a "dynamic equilibrium" regime.





ACPD
10, 30857–30891, 2010